Letters

Cascading Synchronization Instability in Multi-VSC Grid-Connected System

Xikun Fu, Meng Huang, *Member, IEEE*, Shangzhi Pan, *Senior Member, IEEE*, and Xiaoming Zha, *Member, IEEE*

***Abstract*—In this letter, a cascading synchronization instability phenomenon is reported in a multi-voltage-source-converter (VSC) grid. By adopting the equal area criterion, it is revealed that during the fault transient, there is static interaction that increases equivalent mechanical power for the original stable-operating VSC. Due to the fast power angle swing of the unstable VSC, there is nonnegligible dynamic interaction, which may decrease its synchronization stability margin. The effect of system parameters on synchronization stability is studied, and the simulation and experimental results verify the analysis.**

***Index Terms*—Grid-following (GFL) control, interaction, synchronization stability, voltage-source converter (VSC).**

I. Introduction

NOWADAYS, large amounts of renewable energy are connected to the power grid via power electronics converters. The grid-following (GFL) controlled voltage-source converter (VSC) is widely used in the photovoltaic or wind farms due to its simple synchronization mechanism through a phase-locked loop (PLL).

However, the transient synchronization instability risk of GFL-VSC is identified in the literature [1]. During severe grid fault strike, the PLL may lose synchronization since its transient response is fast and nonlinear dynamics. In this regard, many studies are performed to uncover the transient dynamics of the GFL-VSC system. In [1]–[3], the transient stability of a GFL-VSC system is analyzed by equal area criterion (EAC), phase portrait, and energy-based methods. The nonlinear operation mechanism and synchronization boundaries are uncovered.

Practically, in photovoltaic or wind farm applications, a number of VSCs are connected to the ac grid through various transmission lines. Unlike traditional synchronous generators (SGs), the GFL-VSCs may exhibit fast frequency and power angle dynamics in a large range and can become asynchronous.

Manuscript received December 23, 2021; revised January 28, 2022; accepted February 16, 2022. Date of publication February 25, 2022; date of current version March 24, 2022. This work was supported by the National Natural Science Foundation of China under Grant 51877159. *(Corresponding author: Meng Huang.)*

The authors are with the School of Electrical Engineering and Automation, Wuhan University, Wuhan 430072, China (e-mail: xikunfu@whu.edu.cn; meng.huang@whu.edu.cn; shangzhi.pan@whu.edu.cn; xmzha@whu.edu.cn).

Color versions of one or more figures in this article are available at https://doi.org/10.1109/TPEL.2022.3153283.

Digital Object Identifier 10.1109/TPEL.2022.3153283

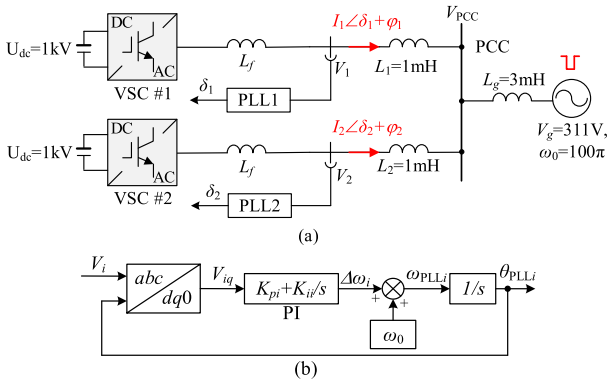

Fig. 1. (a) Two-VSC grid-connected system. (b) Structure of the SRF PLL*i*.

Therefore, the interaction of the asynchronous power sources would be significant.

These kinds of interactions are noticed by researchers for the system containing GFL-VSCs paralleled with SG or grid-forming controlled VSC [4], [5]. But the stability problem of the GFL-VSC is ignored. In a recent work [6], the static synchronization stability level of the multi-VSC system is investigated. A simple impedance-based method is proposed for the stability assessment. However, the dynamic interaction may cause a complex stability problem in such multi-VSC grid-connected systems. In this letter, a cascading synchronization instability is identified. The interaction term of two VSCs is modeled, and the EAC is adopted to find out the synchronization stability margin to prevent cascading failure.

II. Cascading Instability Phenomenon

As shown in Fig. 1(a), two VSCs are connected in parallel to an ac grid at the point of common coupling (PCC). The current control loop is ignored considering its fast response dynamics. The PLL*i* of the VSC #*i* ($i = 1, 2$) generates frequency and phase by following the voltage V_i. L_f represents the filter inductance. L_g and L_i denote the grid and line impedances, respectively. I_i denotes the amplitude of the reference current.

Here, a basic synchronous reference frame (SRF) PLL is adopted in VSCs, as displayed in Fig. 1(b). The phase angle between the output voltage of the VSC #*i* and the grid voltage

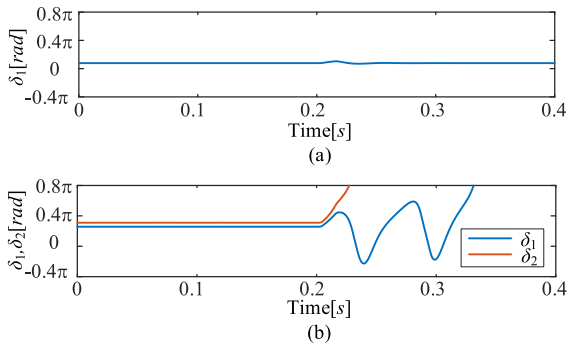

Fig. 2. (a) Stable operation of a single VSC #1 without interaction under grid-side fault. The reference active current of VSC #1 is set as 60 A. (b) Unstable operations of VSC #1 and VSC #2 in parallel with interaction under grid-side fault. The reference active currents of the VSC #1 and VSC #2 are set as 60 A and 160 A, respectively.

is defined as δ_i, i.e.,

$$\delta_i = \theta_{\mathrm{PLL}i} - \theta_g. \tag{1}$$

The $\varphi_i = \tan^{-1}(i_{qi}^{\mathrm{ref}}/i_{di}^{\mathrm{ref}})$ is the angle of the injected current relative to the PLL phase angle. Therefore, the current phase angle of VSC #*i* is $\delta_i + \varphi_i$.

As displayed in Fig. 2(a), a single VSC #1 restores stability after a three-phase voltage dip fault at grid side. It is shown that without interaction influence, the VSC #1 is well-designed and can work stably under a fault strike.

However, when VSC #2 is connected to the PCC, the interaction between VSC #1 and 2 emerges, where the rated current of VSC #2 is set as 160 A. As shown in Fig. 2(b), under the same fault, the VSC #2 loses synchronization and the power angle δ_2 increases dramatically. However, VSC #1 is affected by the unstable VSC #2 and loses synchronization. It is clearly shown that the well-designed VSC #1 is prone to being unstable in this interacting condition. The cascading synchronization instability occurs in this system.

III. Modeling and Synchronization Stability Analysis of the VSC With Interaction

A. Large-Signal Modeling of the VSC With Interaction

As presented in Fig. 1(a), VSC #1 is tied to the ac grid, along with the interaction from VSC #2. The voltage V_1 followed by the PLL1 can be written as follows:

$$V_1 = (L_1 + L_g)\omega_{\mathrm{PLL}1} I_1 + L_g \omega_{\mathrm{PLL}2} I_2 + V_g. \tag{2}$$

$\omega_{\mathrm{PLL}i} \approx \omega_0$ is used since there is a small frequency deviation $\Delta\omega_i$. Then, the voltage V_{1q} on the q-frame of the PLL1 is given as follows:

$$\begin{aligned} V_{1q} = {} & (L_1 + L_g)\omega_0 I_1 \sin(\theta_{\mathrm{PLL}1} + \varphi_1 + \pi/2 - \theta_{\mathrm{PLL}1}) \\ & + V_g \sin(\theta_g - \theta_{\mathrm{PLL}1}) + L_g \omega_0 I_2 \sin(\theta_{\mathrm{PLL}2} + \varphi_2 + \pi/2 \\ & - \theta_{\mathrm{PLL}1}). \end{aligned} \tag{3}$$

As shown in Fig. 1(b), the voltage V_{1q} is used as the input of the proportional–integral (PI) controller of PLL1. Therefore, δ_1 can be written as follows:

$$\delta_1 = \int \left[\left(K_{p1} + K_{i1} \int \right) V_{1q} \right]. \tag{4}$$

When the reference reactive current in the VSCs is 0, $\varphi_{12} = 0$ is obtained. Based on (3) and (4), the second-order differential equation of VSC #1 with interaction from VSC #2 can be found as follows:

$$\begin{aligned} d\delta_1/dt &= \omega_1 - \omega_0 = \Delta\omega_1 \\ d\omega_1/dt &= K_{i1}(L_1 + L_g)\omega_0 I_1 - K_{i1} V_g \sin\delta_1 \\ &\quad - K_{p1} V_g \cos(\delta_1)\Delta\omega_1 \\ &\quad + \underbrace{L_g \omega_0 I_2 [K_{i1} \cos\delta_{21} - K_{p1} \sin(\delta_{21})\Delta\omega_{21}]}_{\text{interaction item}} \end{aligned} \tag{5}$$

where δ_{21} denotes the power angle difference between δ_2 and δ_1, and $\Delta\omega_{21}$ represents the differential of δ_{21}.

According to (5), when the reference active current $I_2 = 0$, the interaction will not emerge in VSC #1. Hence, the difference without and with interaction directly reflects the interaction item from VSC #2, i.e.,

$$L_g \omega_0 I_2 [K_{i1} \cos\delta_{21} - K_{p1} \sin(\delta_{21})\Delta\omega_{21}]. \tag{6}$$

B. Comparison With the SG

First, the swing equation of the SG can be expressed as follows:

$$\begin{aligned} d\delta/dt &= \omega - \omega_0 = \Delta\omega \\ d\omega/dt &= (P_M - P_E - D\Delta\omega)/T_J \end{aligned} \tag{7}$$

where δ represents the power angle; P_M and P_E indicate the mechanical and electromagnetic powers, respectively; T_J denotes the inertial time constant; and D is the damping coefficient.

It is found that the nonlinear model of VSC #1 without interaction is similar to the SG model (7). According to the expression in (5), it is obtained that the equivalent mechanical power $P_{M1} = K_{i1}(L_1 + L_g)\omega_0 I_1$, the electromagnetic power $P_{E1} = K_{i1} V_g \sin\delta_1$, the inertial time constant $T_{J1} = 1$, and the damping coefficient $D_1 = K_{p1} V_g \cos\delta_1$.

However, when mutually synchronous VSCs are met, namely, $\Delta\omega_2 - \Delta\omega_1 = 0$, the power angle difference δ_{21} between VSCs #2 and #1 is invariable. There will be a static interaction item, which can be regarded as the extra mechanical power. Based on (6), the extra mechanical power $P_{\mathrm{inter1}\,e}$ is given as follows:

$$P_{\mathrm{inter1}e} = K_{i1} L_g \omega_0 I_2 \cos\delta_{21e} \tag{8}$$

where $\cos\delta_{21\,e}$ is the steady-state power angle difference.

Moreover, when the mutual asynchronization occurs in the VSCs, $\Delta\omega_2 - \Delta\omega_1 \neq 0$. Thus, the δ_{21} can be given as follows:

$$\delta_{21} = \int (\Delta\omega_2 - \Delta\omega_1) dt + \cos\delta_{21e}. \tag{9}$$

The change in δ_{21} will transform the static interaction into a dynamic interaction, generating a variable P_{inter1}. Referencing to (6) and (8), compared with the static interaction, the dynamic

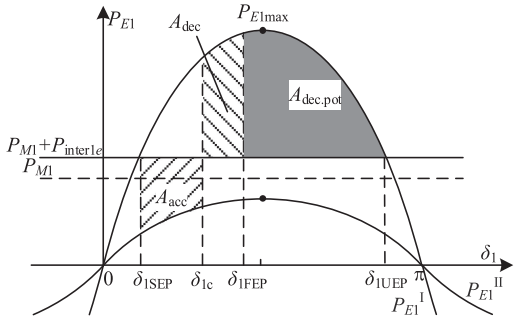

Fig. 3. Effect of the static interaction on the synchronization stability of VSC #1.

interaction will bring a variable mechanical power ΔP_{inter1} to VSC #1, which can be given as follows:

$$\begin{aligned}\Delta P_{\text{inter1}} &= P_{\text{inter1}} - P_{\text{inter1}e} \\ &= L_g\omega_0 I_2\left[\sqrt{{K_{i1}}^2 + {K_{p1}}^2{\Delta\omega_{21}}^2}\cdot\cos(\delta_{21}+\alpha)\right. \\ &\quad \left. - K_{i1}\cos\delta_{21e}\right] \end{aligned} \tag{10}$$

where $\alpha = \tan^{-1}[(K_{p1}\Delta\omega_{21})/K_{i1}]$.

C. Synchronization Stability Analysis

In the EAC method, it is usually assumed that VSC #1 is operating at a stable equilibrium point (SEP) $\delta_{1\text{SEP}}$ before a fault occurs. Then, the power characteristic ${P_{E1}}^{\text{I}} - \delta_1$ curve is switched to the ${P_{E1}}^{\text{II}} - \delta_1$ curve during the fault and returns to ${P_{E1}}^{\text{I}} - \delta_1$ curve when the fault is removed at δ_{1c}. Thus, δ_1 reaches the far endpoint (FEP) $\delta_{1\text{FEP}}$. A_{acc} and A_{dec} are called the acceleration and deceleration areas, respectively. The stability margin η can be expressed as

$$\eta = \underbrace{\int_{\delta_{1c}}^{\delta_{1\text{UEP}}}({P_{E1}}^{\text{I}} - P_{M1})d\delta_1}_{A_{\text{dec}}+A_{\text{dec.pot}}} - \underbrace{\int_{\delta_{1\text{SEP}}}^{\delta_{1c}}(P_{M1} - {P_{E1}}^{\text{II}})d\delta_1}_{A_{\text{acc}}} \tag{11}$$

where the potential deceleration area $A_{\text{dec.pot}}$ exists between the FEP and the unstable equilibrium point (UEP).

For a stable trajectory, $A_{\text{acc}} = A_{\text{dec}}$ is met. The stability margin $\eta > 0$, $A_{\text{dec.pot}} > 0$. It means that VSC #1 needs additional kinetic energy to reach the UEP, making it asynchronous operating. In addition, there exists the maximum $A_{\text{dec.potmax}}$ when $A_{\text{acc}} = 0$. For an unstable trajectory, $A_{\text{dec.pot}} = 0$ is met. $\eta < 0$. It indicates that A_{dec} is not sufficient. The VSC #1 still has kinetic energy at the UEP and, thus, loses synchronization.

$P_{\text{inter1}e} > 0$ represents the static interaction effect by additional mechanical power. As displayed in Fig. 3, the $P_{\text{inter1}e}$ leads to an expanded A_{acc} and a reduced $A_{\text{dec.pot}}$. The stability margin of VSC #1 is shrunk. The static interaction deteriorates the synchronization stability of VSC #1.

Actually, the interaction is dynamic due to an unavoidable oscillation of δ_{21}, resulting in a varying P_{inter1}. The $P_{E1} - \delta_1$ curve during the increase in δ_1 is shown in Fig. 4(a). Compared

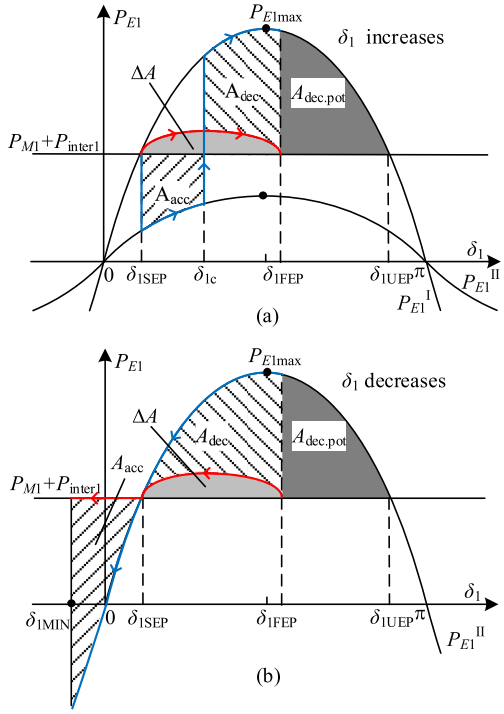

Fig. 4. Effects of the dynamic interaction on the synchronization stability of VSC #1. The increasing and decreasing processes of power angle are shown in (a) and (b), respectively.

with the static interaction, the dynamic interaction by the variable P_{inter1} increases the acceleration area A_{acc} and reduces the deceleration area A_{dec}. Obviously, VSC #1 is injected with the extra energy ΔA, causing the reduction in its stability margin η. That is to say, if the additional energy $\Delta A > 0$ is neglected, the estimated synchronization stability margin of VSC #1 would be overoptimistic.

The $P_{E1} - \delta_1$ curve during δ_1 decreases is shown in Fig. 4(b). With an identical interaction effect, the deceleration of A_{dec} leads to the reduction of A_{acc}, which enhances the stability margin η of VSC #1. In fact, VSC #1 reduces the extra energy ΔA under the interaction process, leading to an improvement of its synchronization stability.

In summary, the stability margin η considering the dynamic interaction can be presented as follows:

$$\eta = A_{\text{dec}} + A_{\text{dec.pot}} - A_{\text{acc}} - \Delta A. \tag{12}$$

Based on (10), the extra energy ΔA from dynamic interaction can be expressed as follows:

$$\Delta A = \int \Delta P_{\text{inter1}} d\delta_1 = \int \Delta P_{\text{inter1}}\Delta\omega_1 dt. \tag{13}$$

When $\Delta P_{\text{inter1}}\Delta\omega_1 > 0$ is satisfied, the dynamic interaction will always weaken the synchronization stability of VSC #1. It should be noted that due to the injection of additional energy ΔA, the power flow balance of the potential and kinetic energies in VSC #1 is broken. Therefore, VSC #1 is not a conservative energy system, and there is no guarantee that the first-swing stable VSC #1 will restore synchronization stability.

TABLE I
COMPARISON OF SYNCHRONOUS STABILITY

Case	$A_{\text{dec.potmax}}$	$A_{\text{dec.pot}}$	$\Delta A_{\max}$	$\eta_{\min} = A_{\text{dec.pot}} - \Delta A_{\max}$
1	0.28	0.19	0	0.19
2	0.28	0.19	$0.96\times(\delta_{1\text{FEP}}-\delta_{1\text{MIN}})$	$0.19-0.96\times(\delta_{1\text{FEP}}-\delta_{1\text{MIN}})$

According to (10), the maximum mechanical power $\Delta P_{\text{inter1max}} \approx 0$ when δ_1 increases to $\delta_{1\text{FEP}}$, which makes the extra energy ΔA unchanging or decreasing. Conversely, the minimum mechanical power $\Delta P_{\text{inter1min}} \approx -2K_{i1}L_g\omega_0 I_2$, which causes the extra energy ΔA to increase rapidly when δ_1 decreases from $\delta_{1\text{FEP}}$ to the minimum point $\delta_{1\text{MIN}}$. Thus, the maximum extra energy $\Delta A_{\max}$ in one swing cycle is given as follows:

$$\Delta A_{\max} = \int_{\delta_{1\text{FEP}}}^{\delta_{1\text{MIN}}} \Delta P_{\text{inter1min}} d\delta_1 . \tag{14}$$

IV. VERIFICATION

The system in Fig. 1 with two VSCs connecting to an ac grid is built in the MATLAB/Simulink and experimental platform. The reference active currents I_1 and I_2 are 60 A and 160 A, respectively. The operation condition is that a three-phase grounded fault occurs and the grid voltage V_g drops to 0.8 (p.u.) at 0.1 s and lasts for 0.013 s.

The normalized values (in p.u.) of $P_{E1\max}$, P_{M1}, and $P_{\text{inter1}e}$ based on the reference value $K_{i1}V_g$ in the pre- and midfault are 1.00, 0.24, 0.48 and 0.80, 0.24, 0.48, respectively. The $\delta_{1\text{FEP}}$ can be estimated as 1.40 rad.

In *Case*1, the power angle difference δ_{21} is controlled as constant, leading to only static interaction existing in VSC #1, i.e., $\Delta P_{\text{inter}} = 0$. In *Case*2, the power angles δ_1 and δ_2 are independently controlled by PLL1 and PLL2, respectively, leading to dynamic interaction being affected by the variable δ_{21}, and $\Delta P_{\text{inter1min}} = -0.96$ is obtained.

The theoretical calculation results are shown in Table I. $A_{\text{dec.pot}}$ in both *Case* 1 and *Case* 2 is 0.19 when meeting the same fault. With extra energy $\Delta A_{\max} = 0$ in *Case*1, VSC #1 restores to the SEP. However, an additional energy $\Delta A > 0$ in *Case*2 is present. When $\Delta A_{\max} > A_{\text{dec.pot}}$ is satisfied, the interaction makes the VSC #1 cross the UEP and thus destabilized.

Fig. 5 shows the transient processes of the VSCs in *Case*1 and *Case*2. In Fig. 5(a), the unbalanced power under the fault generates an acceleration process of δ_1 and VSC #1 has $A_{\text{dec.pot}} = 0.19$. $\Delta A = 0$ is achieved by a constant power angle difference in control. Thus, $\eta = 0.19$ suggests that VSC #1 does not have enough energy to reach UEP.

Fig. 5(b) shows that VSC #2 loses synchronization after the fault. With the interaction influence of the destabilized VSC #2, the extra energy $\Delta A = 1.9$ is injected into VSC #1, which is more than $A_{\text{dec.pot}} = 0.19$. Thus, VSC #1 has kinetic energy at the UEP, and its synchronization stability is lost. In addition, $\eta < 0$ reveals that there is kinetic energy at UEP in each cycle. Hence, VSC #1 cannot recover synchronous operation after the fault.

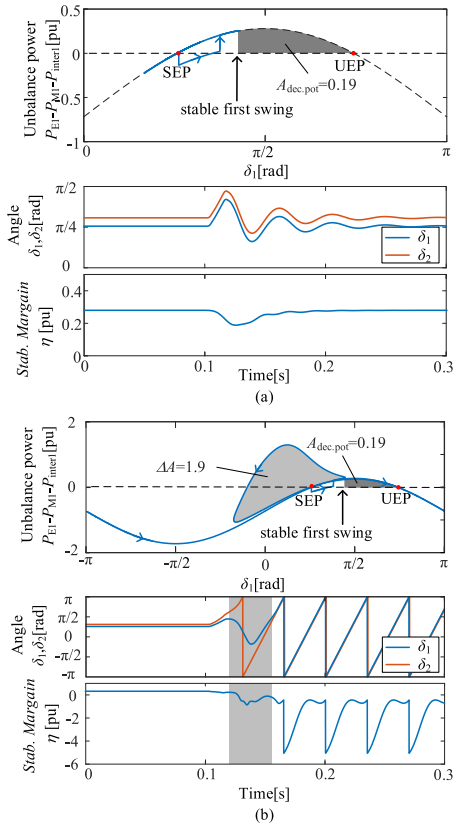

Fig. 5. Grid-side voltage dip fault occurs at 0.1 s and lasts for 0.013 s. The VSC #1 is stable and unstable when *Case* 1 is met in (a) and *Case* 2 is met in (b), respectively. (a) Constant power angle difference is controlled. (b) Varying power angle difference in the shaded region.

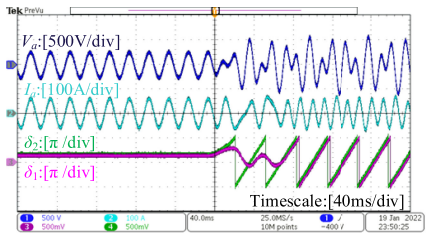

Fig. 6. Response of the VSCs in parallel under the voltage dip fault.

The simulations demonstrate that VSC #1 is originally stable in *Case* 1 and suffers from cascading instability in *Case* 2. Compared with static interaction in *Case* 1, the dynamic interaction in *Case* 2 injects extra energy into VSC #1, driving the first-swing stable VSC #1 to lose its synchronization. The results also illustrate that VSC #1 under the interaction is not a dissipative energy system.

Case 2 is established in the experimental bench with a three-phase grid voltage dip to 0.85 (p.u.). Fig. 6 clearly shows a cascading instability in this two-VSC system. Although VSC #1 is stable in its first swing process, it loses synchronous stability when affected by VSC #2, which is unstable after the fault.

To improve the synchronization stability of VSC #1 in *Case* 2, increase $A_{\text{dec.pot}}$ by reducing the injected active power in *Case* 3 and improve the inertia and damping by the increasing K_{p1}

TABLE II
SYNCHRONOUS STABILITY UNDER DIFFERENT PARAMETERS

Case	I_1(A)	K_{p1}/K_{i1}	δ_{FEP} (rad)	$\eta_{\min} = A_{\text{dec.pot}} - \Delta A_{\max}$
2	60	0.4/70	unstable	< 0
3	20	0.4/70	1.74	$0.10 > 0$
4	60	0.6/50	1.81	$0.08 > 0$

and decreasing K_{i1} of the PLL1 in *Case* 4. As shown in Table II, even under the influence of the destabilized VSC #2, VSC #1 still does not cross the UEP in *Case* 3 and *Case* 4.

V. CONCLUSION

A cascading instability of the GFL-VSCs in a grid-connected system is studied in this letter. The GFL converter will suffer from the interaction effects of other converters at PCC. Applying the EAC, it is revealed that the interaction from the other converters changes the equivalent machinal power for the SG-like energy system of the GFL converter, leading to the deterioration of the synchronization stability. However, the released energy from the dynamic interaction will break the energy flow balance in the GFL converter with static interaction, especially in the case of cascading instability, which results in an overoptimistic estimation of the synchronization stability. Theoretical calculation and experimental results verify the above-mentioned analysis.

REFERENCES

[1] X. He, H. Geng, R. Li, and B. C. Pal, "Transient stability analysis and enhancement of renewable energy conversion system during LVRT," *IEEE Trans. Sustain. Energy*, vol. 11, no. 3, pp. 1612–1623, Jul. 2020.

[2] H. Wu and X. Wang, "Design-oriented transient stability analysis of PLL-synchronized voltage-source converters," *IEEE Trans. Power Electron.*, vol. 35, no. 4, pp. 3573–3589, Apr. 2020.

[3] X. Fu *et al.*, "Large-signal stability of grid-forming and grid-following controls in voltage source converter: A comparative study," *IEEE Trans. Power Electron.*, vol. 36, no. 7, pp. 7832–7840, Jul. 2021.

[4] J. Choi, M. S. Illindala, A. Mondal, A. A. Renjit, and M. C. Pulcherio, "Cascading collapse of a large-scale mixed source microgrid caused by fast-acting inverter-based distributed energy resources," *IEEE Trans. Ind. Appl.*, vol. 54, no. 6, pp. 5727–5735, Nov./Dec. 2018.

[5] C. Shen *et al.*, "Transient stability and current injection design of paralleled current-controlled VSCs and virtual synchronous generators," *IEEE Trans. Smart Grid*, vol. 12, no. 2, pp. 1118–1134, Mar. 2021.

[6] X. He and H. Geng, "PLL synchronization stability of grid-connected multi-converter systems," *IEEE Trans. Ind. Appl.*, vol. 58, no. 1, pp. 830–842, Jan./Feb. 2022.